Dysregulated Skeletal Muscle Myosin Super-relaxation in Type II, but Not Type I, Diabetes Mellitus

Christopher T. A. Lewis[1], Roger Moreno-Justicia[2], Lola Savoure[1], Enrique Calvo[3,12], Agata Bak[3], Jenni Laitila[1], Robert A.E. Seaborne[1,4], Steen Larsen[1, 5], Hiroyuki Iwamoto[6], Marina Cefis[7], Jose A. Morais[8], Gilles Gouspilou[8], Jorge Alegre-Cebollada[3], Thomas J. Hawke[9], Jesús Vazquez[3,12], Miquel Adrover[10], Vincent Marcangeli[11], Atul S. Deshmukh[2], Julien Ochala[1,3]*

[1]Department of Biomedical Sciences, University of Copenhagen, Copenhagen, Denmark

[2]Novo Nordisk Foundation Center for Basic Metabolic Research, Faculty of Health and Medical Sciences, University of Copenhagen, Denmark.

[3]Centro Nacional de Investigaciones Cardiovasculares (CNIC), Madrid, Spain.

[4]Centre for Human and Applied Physiological Sciences, Faculty of Life Sciences & Medicine, King's College London, London, UK.

[5]Clinical Research Centre, Medical University of Bilalystok, Bialystok, Poland

[6]Spring-8, Japan Synchrotron Radiation Research Institute, Hyogo, Japan.

[7]Département des Sciences de l'Activité Physique, Faculté des Sciences, UQAM, Montréal, Québec, Canada.

[8]Department of Medicine, Research Institute of the McGill University Health Centre, Montréal, Québec, Canada.

[9]Department of Pathology and Molecular Medicine, McMaster University, Hamilton, Ontario, Canada.

[10]Institut Universitari d'Investigació en Ciències de la Salut (IUNICS), Institut d'Investigació Sanitària Illes Balears (IdISBa), Departament de Química, Universitat de les Illes Balears, Palma de Mallorca,

Spain.

[11]Département des sciences biologiques, Faculté des Sciences, UQAM, Montréal, Québec, Canada.

[12]CIBER de enfermedades cardiovasculares (CIBERCV), Madrid, Spain

Corresponding author: Julien Ochala

Address: Panum Institute, Blegdamsvej 3B, 2200, Copenhagen, Denmark

ORCID ID: 0000-0002-6358-2920

Email: julien.ochala@sund.ku.dk

Conflicts of interest: CTAL is an employee at Novo Nordisk A/S. The work of this paper was performed prior to beginning this position and the conclusions drawn from this manuscript are in no way influenced by their current position.

Abstract

Skeletal muscle plays a critical role in the onset and development of type II diabetes. However, very few studies have investigated the potential pathogenic role of its most abundant protein, myosin. Hence, here, we aim to define this by focusing on myosin energy-saving state known as super-relaxed state (SRX). We performed an array of (loaded Mant-ATP chase experiments, LC-MS/MS proteomics, X-ray diffraction) assays on *vastus lateralis* biopsies from diabetic patients and matched controls. Strikingly, our results highlight that the amount of muscle myosin molecules in SRX is higher and the related ATP demand lower in type II diabetes patients than in controls. These physiological changes are parallel with greater glycation levels on myosin heavy chains, and with remodeled sarcomeric proteins in the same type II diabetes patients. None of these (mal)adaptations were noticed in patients with type I diabetes. Altogether, our findings emphasize a complex molecular dysregulation of myosin SRX and ATP consumption in type II diabetes. Ultimately, pharmacological targeting of SRX could benefit whole-body metabolic health through the enhancement of energy expenditure.

Introduction

As a major tissue in the regulation of whole-body glycemic control, skeletal muscle has long been established as critical to the development and onset of type 2 diabetes mellitus (T2DM) [1]. Whilst decades of research have advanced our molecular understanding of how skeletal muscle contributes to the etiology of such disease, few of these studies have investigated molecular changes in energy expenditure and whether the most fundamental contractile unit of muscle, the sarcomere, is involved.

The sarcomere is the repeating unit of striated muscle which facilitates the coordinated contraction of muscle via interactions between the myosin and actin filaments [2,3]. The contraction of striated muscle is highly energy-dependent, and ATP is consumed directly by the head region of the myosin molecule, which is itself an ATPase [4,5]. Until recently, energy usage by the sarcomere was thought to be mostly linked to the consumption of ATP by the myosin molecule during muscular contraction [6]. However, this doctrine has been challenged following the discovery that myosin maintains a significant consumption of ATP, and that the rate of this ATP consumption is dependent on its resting conformation [7]. It is now established that myosin can adopt at least two different biochemical states at rest, known as the disordered-relaxed state and the super-relaxed state [7-9]. In the disordered-relaxed state (DRX), the myosin heads are likely to be in a structural ON state. They are not bound to actin and can exist freely in the interfilamentous space of the sarcomere [10-12]. In the super-relaxed state (SRX), the head regions of the myosin molecules have a structural OFF conformation in which they are folded backwards against the thick filament backbone of the sarcomere [11,13-15]. This folding means that in the SRX state, the ATPase site located on the head region of the myosin molecule is sterically inhibited, preventing ATP binding [12,16]. Therefore, myosin molecules which are in SRX, have an ATP turnover rate which is approximately ten times slower than those in DRX [8,17,18].

The myosin molecules within each striated muscle fiber exist in a carefully controlled ratio of DRX:SRX [19]. It has been demonstrated that dysregulation of this ratio is pathogenic in genetic diseases [13]. This occurs in inherited conditions of both cardiac and skeletal muscle following mutations to genes encoding proteins of the sarcomere [20-25]. It has also been estimated that a 20% shift of myosin heads from SRX to DRX in skeletal muscle would increase whole-body energy expenditure by 16% [8]. Following these studies, uncovering potential changes to the DRX:SRX ratio in metabolic diseases, such as T2DM, is of great interest as it would unravel major molecular disturbances in the energy demand. Hence, in the present study we aimed to explore the hypothesis that, in T2DM, there would be a re-modelling of the proportions of myosin molecules in DRX and SRX ultimately affecting the ATP consumption of resting skeletal muscle.

The main cellular source of ATP is glycolysis, a process that is not harmless for cells, as it produces highly reactive carbonyl compounds as side products. The most important one is methylglyoxal (MG), an α-oxo-aldehyde whose concentration in cells and tissues is typically 2-4 μM. Despite of that, its high intrinsic reactivity (~50,000 times higher than that of glucose) makes it one of the endogenous compounds with higher ability to randomly modify nucleophilic groups of long-life biomolecules [26-29]. Because of that, evolution has designed enzymatic mechanisms to control the levels of intracellular MG, such as the glyoxalase system (Glo-1 and Glo-2). However, both enzymes become downregulated under diabetes mellitus and consequently, the levels of MG in diabetic patients are 2 to 6-fold higher than in healthy people [30-32]. Once it is formed, MG rapidly reacts with Arg, Lys and Cys side-chains producing MG-derived advanced glycation end-products (AGEs), such as N^{ε}-(carboxyethyl)lysine (CEL), hydroimidazolones (MG-Hs; which include MG-H1, MG-H2 and MG-H3) or 2-ammonio-6-[1-(5-ammonio-6-oxido-6-oxohexyl)-5-methylimidazolium-3-yl] hexanoate (MOLD) that involves the covalent crosslinking of two Lys [33-36]. The formation of these AGEs changes the chemical nature of the protein residues, thus potentially impacting the protein structure and the function and therefore, exacerbate the progression of T2DM, particularly in the microvasculature [37].

Some recent studies have demonstrated that in patients with T2DM, glycation can also occur on proteins of the cardiac sarcomere, including myosin, thus impacting their function [38-40]. Sarcomeric proteins may be of particular susceptibility to glycation during metabolic diseases due to their relatively long half-life [41]. Thus, here, we further aimed to test the hypothesis that changes in the myosin DRX:SRX ratio in T2DM would intrinsically be caused by aberrant levels of glycation. We investigated all these by isolating individual skeletal muscle fibers from the *vastus lateralis* of male patients with T2DM and controls, who were matched for age, body-mass index (BMI) and physical activity levels (Table 1).

Results

Patients with T2DM have higher levels of myosin SRX/OFF state in type I muscle fibers.

To directly test our hypothesis that myosin DRX to SRX ratio could be altered in patients with T2DM, we performed loaded Mant-ATP chase assays on isolated and permeabilized single muscle fibers (Figure 1a). A total of 284 individual myofibers were tested (between 8 and 12 fibers per individual). A fiber type breakdown from these samples is shown (Table 1). Interestingly, we found a significantly lower number of myosin heads in DRX (P1) in type I fibers of T2DM patients than in controls (Figure 1b). This finding was matched by a significantly higher percentage of fibers in SRX (P2) in type I fibers of T2DM patients than in controls (Figure 1c). Despite these, we did not observe any differences between the groups in the ATP turnover times of the myosin molecule in DRX (T1) (Figure 1d) or SRX (T2) (Figure 1e). These results demonstrate that in T2DM, resting myosin state undergoes remodeling causing a decrease in the ATP consumption of type I, oxidative, fibers.

To gain further structural insights and relate the above DRX/SRX with myosin ON/OFF states, we performed small-angle X-ray diffraction on the same muscle biopsy specimens and focused on myosin meridional reflections, namely M3 and M6 (Figure 1f). We found that the M3 intensity (not spacing) was significantly greater in T2DM patients than in controls (Figure 1g-h). This suggests that, even though the distance between myosin crowns is preserved, there is a higher order of myosin heads along the thick filament (OFF state) [42]. We did not observe any change in M6 intensity or spacing between the groups (Figure 1i-j), highlighting the maintenance of thick filament compliance/extensibility [42]. Altogether, our findings support that, in type I fibers of T2DM patients, myosin molecules adopt a preferred ATP-conserving SRX and OFF state without any other major thick filament disturbances.

Preserved myosin resting states in myofibers of individual with genetic T1DM.

Following the above results in T2DM, we sought to examine whether these alterations were specific to this condition or whether they also occurred with type 1 diabetes mellitus (T1DM). We tested isolated skeletal muscle fibers from the *vastus lateralis* of patients with T1DM and controls, who were matched for sex, age, BMI and fiber type breakdown (Table 2). Once again, we applied loaded Mant-ATP chase experiments (Figure 2a). A total of 104 individual myofibers were evaluated (between 8 and 12 muscle fibers per participant). Unlike T2DM, we found no significant difference in the proportion of myosin molecules in DRX or SRX between T1DM patients and controls (Figure 2b-c). Similarly, the ATP turnover time of myosin heads in DRX or SRX were not group-dependent (T1 and T2, Figure 2d-e).

In addition to DRX/SRX, to verify that the myosin ON/OFF states were not altered in T1DM, we applied the small-angle x ray diffraction technique on the same samples (Figure 2f). As expected, no changes in M3 intensity or spacing were noted (Figure 2g-h). Similarly, no differences were found in M6 intensity or spacing (Figure 2i-j). Together, our results indicate that, unlike T2DM, T1DM is not associated with any change in myosin SRX/OFF state in any fiber type.

The coiled coil domain of the *MYH7* protein is glycated in individuals with T2DM.

To get a deeper understanding of the molecular events leading to the changes in myosin resting states, we focused on post-translational modifications, more specifically on glycation, known to be highly prevalent in T2DM. A graphical schematic illustrates the formation of MG and the formation of MG-derived AGEs (Figure 3a). Analyzing by LC-MS/MS the peptides derived from the digestion of SDS-PAGE-separated protein bands, we identified several AGE-modified peptides arising from the myosin heavy chain type I (*MYH7*) protein obtained from T2DM patients (Figure S1), which were absent in the controls (Figure 3b). The identification of these glycated peptides was in-depth validated by a highly sensitive scan using the VseqExplorer application to calculate quantitative E-

scores (see Materials and Methods). These glycated peptide fragments were mainly located upon the coiled coil region of the *MYH7* protein (Figure 3b-c), and we could detect the formation of some MG-derived AGEs on them (mainly CEL and MG-Hs).

Acute glycation of type I muscle fibers induces an increase of the percentage of resting myosin heads in SRX.

To emphasize the functional effects of glycation on myosin proteins, we performed paired loaded Mant-ATP chase experiments with and without MG after 30-minute incubation (Figure 4a). A total of 37 isolated muscle fibers were tested. Consistent with our previous results, the baseline percentage of myosin heads in DRX was lower in type I muscle fibers of T2DM patients than in controls (Figure 4b). This was matched with a greater proportion of SRX in type I muscle fibers of T2DM patients than in controls (Figure 4c). Following incubation with MG, the fraction of myosin heads in DRX of type I fibers from controls significantly decreased but not of type II fibers (Figure 4b). Again, this was matched with a significant increase in the amount of SRX in type I fibers of controls but not in type II fibers (Figure 4c). Conversely, we did not find any change following MG incubation in either fiber type in T2DM patients (Figure 4b-c). A plausible reason for such discrepancy is likelihood that fibers from T2DM patients were already saturated and hyper-glycated at the time of the baseline experiments. MG incubations also had an impact on the ATP turnover time of the resting myosin molecules (Figure 4d-e).

Differential expression of sarcomeric proteins in type I muscle fibers of patients with T2DM.

Besides post-translational modifications and glycation, other more profound remodelling may occur in T2DM and may include alterations in skeletal muscle protein expression, especially within type I muscle fibers where we observed most of the above changes [43]. To investigate this, we performed high-throughput single muscle fiber proteomics using the same muscle biopsy specimens (Figure 5a). A total of 109 single muscle fibers were analyzed from 10 different muscle biopsies (5/group). On an

average 584 proteins were quantified in each single muscle fiber (Supplementary table 1). The samples were grouped by fiber type as determined by immunohistochemistry, which was validated by the proteomics data. The validation revealed expected enrichment of known type I or II fiber specific proteins, such as TNNT1 and TNNI1 or MYH2 and MYBPC2 respectively (Figure 5b). This validation of the method via the examination of expression profiles between fiber types provided a high level of confidence to proceed and look at the specific changes between the control and T2DM groups in each individual fiber type.

Interestingly, in type I muscle fibers, we identified 136 differentially expressed proteins between controls and T2DM patients. Importantly, a large amount of sarcomeric proteins such as MYLK2, MYBPC2 and MYL4 were downregulated in T2DM muscle fibers (Figure 5c, Supplementary table 1). On the other hand, in type II myofibers, controls and T2DM patients exhibited we observed 32 differentially expressed proteins between controls and T2DM group. Among these, mitochondrial-associated proteins, such as NDUFS5, NDUFA10 and NDUFS8 were downregulated in T2DM (Figure 5d, sup table x). Notably, four proteins were upregulated by T2DM in both type I and type II muscle fibers, including the peroxisomal protein ECH1. In summary, our analysis revealed distinct patterns of protein expression changes in type I and type II muscle fibers between control and T2D patients.

Discussion

In the present study, we aimed to identify whether resting myosin biochemical and structural states were altered in T2DM. We observed a higher proportion of myosin heads in SRX and OFF state in T2DM patients than in controls. Interestingly, these alterations were only present in type I, slow oxidative, muscle fibers and were not found in T1DM patients. The exact mechanisms underlying the increase in myosin super-relaxation may be complex but are likely to involve T2DM-specific hyper-glycated residues on the coiled coil region of myosin heavy chain type I (*MYH7*). Indeed, when acute hyper-glycation was induced in isolated single muscle fibers, the percentage of myosin heads in SRX increased. Besides a hyper-glycation, myosin super-relaxation in T2DM may also involve a remodelling of sarcomeric proteins as revealed by our single fiber proteomics analyses.

The discovery of SRX has remarkably shifted the field of muscle cell biology and has implied a potential direct link between resting myosin conformation and the metabolic rate of skeletal muscle [7,8]. However, much of the early work on resting myosin head biophysics has been concentrated on cardiac diseases and in particular, hypertrophic cardiomyopathy, an inherited disease caused by mutations to sarcomeric proteins [13,20-23]. It is only recently that we have demonstrated that myosin biochemical states are dynamic and greatly influenced by non-genetic factors [44,45]. Thus, based on these findings, investigating the potential involvement of changes to the dynamics of myosin in cardiometabolic syndromes such as T2DM was an obvious next step.

Our main finding, a higher fraction of myosin molecules in SRX and OFF state in T2DM, is striking. Critically, this means that the type I fibers of patients with T2DM have a reduced ATP turnover and thus energy consumption per muscle fiber. As skeletal muscle makes up around 40% of whole-body mass, even small changes in the energy consumption of this tissue can have significant consequences for whole-body energy expenditure [46]. This is particularly interesting as patients with T2DM have been demonstrated to lose weight to a lesser extent than overweight, non-diabetic, controls, even

when placed on matched weight management interventions [47,48]. Future studies in this field should focus on the whether resting myosin SRX/OFF state is altered in obesity without the background of T2DM and whether dynamic changes to myosin conformation occur following weight loss and/or gain. Based on all these findings, it is tempting to suggest that restoring SRX in the context of metabolic syndromes would promote ATP consumption at the muscle fiber level and may favour a greater whole-body energy expenditure. This would then position myosin as a promising target for alleviating the burden of T2DM. Pharmacological compounds which can directly increase the DRX, specifically in skeletal muscle, may therefore hold therapeutic potential. Of particular interest is the piperine, the main alkaloid component of black pepper, which was demonstrated to be able to induce this effect [49,50]. It is important for future studies to investigate if differences in the myosin conformation exist between sexes as in the present study on male subjects were included in the T2DM patient cohort. This is of particular importance when considering that it has been shown that estradiol is able to disrupt the SRX [51].

Interestingly, in the present manuscript, the higher myosin super-relaxation only occurred in type I muscle fibers. Type I and type II fibers differ metabolically, with type I having a higher density of mitochondria and thus favoring oxidative respiration, whilst type II fibers have a relatively higher glycolytic capacity [52,53]. Importantly, type I muscle fibers have a higher expression of the GLUT4 glucose transporter and have a far higher glucose handling capacity compared to type II fibers [54-56]. Considering that glucose handling of skeletal muscle is one of the critical processes to be dysregulated during the development of T2DM; and that T1DM patients do not have any compromised myosin SRX/OFF state, we believe that delineating whether myosin conformation and glucose handling in T2DM are biologically linked would be essential to pursue in future studies.

As mentioned previously, the exact molecular mechanisms underlying the changes in resting myosin conformations may be complex, but our study highlights the potential role of post-translational

modifications such as glycations. Previous studies from Papadaki *et al.,* showed that in T2DM patients, proteins of the cardiac myofilament were hyper-glycated, and that could reduce cardiac contractility [38,39]. In the SRX/OFF state, the myosin head is folded backwards and thus able to form interactions with this particular region [11,13,14,57,58]. The functional and experimental relevance of these unusual post-translational modifications was demonstrated using MG, the main glycating agent generated in the intracellular space [59,60]. When skeletal muscle fibers were treated with MG, we only observed an increased amount of myosin heads in the SRX state for type I muscle fibers of controls (not for T2DM). It is then highly plausible that, as a non-reversible covalent attachment of a carbohydrate or an α-oxo-aldehyde to an amino acid residue, the MG-treated myofibers from T2DM patients were already glycated/saturated prior to the incubation and thus were not significantly affected [37,61,62].

The proteomics analysis displayed differences in the expression of major sarcomeric proteins in type I skeletal muscle fibers of T2DM. Downregulated proteins included MYL4 and MYLK2. MYL4, myosin essential light chain, is a protein which has ectopic expression in the atria and of the embryonic heart, with functions in increasing Ca^{2+}-sensitivity and then molecular and cellular force production [63,64]. Mutations in its gene are associated with atrial heritable cardiomyopathies [65]. MYLK2 is a kinase which in adults is expressed specifically in skeletal muscle, although inherited pathogenic mutations to its associated gene lead to cardiomyopathies [66]. Interestingly, a decreased expression in MYLK2 has previously been reported in individuals with higher levels of insulin sensitivity compared to individuals with low insulin sensitivity [67]. Future investigation into whether MYLK2 plays a functional role in the regulation of resting myosin conformation is essential, particularly due to the high level of regulation of myosin by PTMs. As a skeletal muscle specific protein, MYLK2 could be a promising target for the modulation of resting myosin states in T2DM and metabolic disease in a way which would not impact the adult heart.

In our analysis of type II fibers, we did not observe changes to sarcomeric proteins. Instead, type II fibers demonstrated differential expression of proteins more traditionally associated with metabolic disease, such as proteins of mitochondria. In particular we observed significant changes to the expression of NADH:ubiquitone oxioreductase subunit proteins, including NDUFS8, NDUFS5 and NDUFA10. These proteins are subunits of NADH dehydrogenase in the mitochondria inner membrane, also known as complex I [68]. This protein converts NADH into NAD^+ within the electron transport chain and is thus vital in the generation of ATP [69]. Interestingly, these proteins have been previously demonstrated to be differentially expressed in the skeletal muscle of patients with T2DM [70,71]. Although, this is the first time in which single fiber proteomics has been utilized in the investigation of T2DM and thus we have been able to identify that these proteins have specifically altered expression in type II fibers. Future experiments with fiber type specific investigation of oxidative phosphorylation in individuals with and without T2DM would be of benefit to the field as it would help define whether mitochondrial dysfunction is fiber type specific in T2DM.

Conclusion

Our findings indicate that T2DM patients undergo a remodelling of their resting myosin SRX/OFF state in type I muscle fibers, leading to a lower ATP demand. Such (mal)adaptation may be related to aberrant glycation levels on myosin heavy chains and may also be related to changes in the expression of sarcomeric proteins. These changes offer promising avenues for drug discovery and development as they mean that if myosin biochemical and structural states were to be targeted pharmacologically and restored in T2DM, they would potentially help increasing the overall muscle/whole-body ATP consumption and thereby promote metabolic health.

Methods

Sample Collection

Human *vastus lateralis* biopsies were collected from three different studies. The collection of muscle biopsies from T2DM participants in Denmark was approved by the ethical committee for the Capital Region of Denmark (H-15010122) and was conducted in accordance with the declaration of Helsinki. All study participants were informed and signed a consent from before enrollment in the study. Characteristics from this study have been previously published and the biopsy procedure is described [72]. For the collection of T2DM muscle biopsies in Canada, all procedures were approved by the Ethics Committee of the Université du Québec à Montréal (CIEREH-2020-3477). Informed consent was obtained from all participants. Skeletal muscle biopsy samples were obtained from the vastus lateralis muscle using a suction modified Bergström needle performed under local anesthesia**.** Samples were immediately frozen in liquid nitrogen and stored at -80C until use. For T1DM patients, skeletal muscle biopsy samples were obtained from the vastus lateralis muscles of control (2 women/3 men; mean age 54±7.3 years old; BMI 24.6±1.4) and T1DM individuals (2 women/3 men; mean age 53±4.6 years old; BMI 25.3±3.1) using a suction modified Bergström needle performed under local anesthesia. The study was reviewed and approved by the Hamilton Integrated Research Ethics Board (HiREB #5344), in accordance with the Declaration of Helsinki. All participants gave verbal and written informed consent. Samples were immediately frozen in liquid nitrogen and stored at -80C until use.

Single muscle fiber preparation

Cryopreserved muscle samples were dissected into small sections and immersed in a membrane-permeabilizing solution (relaxing solution containing glycerol; 50:50 v/v) for 24 hours at -20°C, after which they were transferred to 4°C. As previously published, the relaxing solution contained 4 mM Mg-ATP, 1 mM free Mg^{2+}, 10-6 mM free Ca^{2+}, 20 mM imidazole, 7 mM EGTA, 14.5 mM creatine phosphate and KCl to adjust the ionic strength to 180 mM and pH to 7.0 [25,73]. Additionally, the rigor

buffer for Mant-ATP chase experiments contained 120 mM potassium acetate, 5 mM magnesium acetate, 2.5 mM K_2HPO_4, 50 mM MOPS, 2 mM DTT at pH of 6.8. These bundles were kept in the membrane-permeabilizing solution at 4°C for another 24 hours. After these steps, bundles were stored in the same buffer at -20°C for use up to two weeks [74,75].

Mant-ATP chase assay

Permeabilized skeletal muscle bundles were transferred to the relaxing solution and individual muscle fibers were isolated. Their ends were individually clamped to half-split copper meshes designed for electron microscopy (SPI G100 2010C-XA, width, 3 mm), which had been glued to glass microscopy slides (Academy, 26 x 76 mm, thickness 1.00-1.20 mm). Cover slips were then secured to the top of the slide to create a flow chamber (Menzel-Gläser, 22 x 22 mm, thickness 0.13-0.16 mm)[44,73]. Subsequently, at 20°C, myofibers with a sarcomere length of 2.00 µm were surgically mounted onto the copper mesh (assessed using the brightfield mode of a Zeiss Axio Scope A1 microscope). Each muscle fiber was first incubated for five minutes with a rigor buffer. A solution containing the rigor buffer with added 250 µM Mant-ATP was then flushed and kept in the chamber for five minutes. At the end of this step, another solution made of the rigor buffer with 4 mM ATP was added with simultaneous acquisition of the Mant-ATP chase.

For fluorescence acquisition, a Zeiss Axio Scope A1 microscope was used with a Plan-Apochromat 20x/0.8 objective and a Zeiss AxioCam ICm 1 camera. Frames were acquired every five seconds with a 20 ms acquisition/exposure time using at 385 nm, for five minutes. The mean background fluorescence intensity was subtracted from the average of the fiber fluorescence intensity for each image. Each time point was then normalized by the fluorescence intensity of the final Mant-ATP image before washout (T = 0). These data were then fit to an unconstrained double exponential decay using Graphpad Prism 9.0:

$$\text{Normalized Fluorescence} = 1 - P1\,(1-\exp(-t/T1)) - P2\,(1-\exp(-t/T2))$$

Where P1 (DRX) is the amplitude of the initial rapid decay approximating the disordered-relaxed state with T1 as the time constant for this decay. P2 (SRX) is the slower second decay approximating the proportion of myosin heads in the super-relaxed state with its associated time constant T2 [73]. Mant-ATP Chase Experiments were performed at ambient lab temperature (20°C) for all samples.

All these samples were obtained from individuals having a mixture of myosin heavy chains (MyHCs) in their skeletal muscles. Hence, subsequently to the Mant-ATP chase protocol, each isolated myofiber was stained with a *MYH7* antibody (specific to type I MyHC) to decipher if the fiber was either a type I or type II fiber. Comparisons between muscle fibers sampled from different patient groups were then separated accordingly. Fiber-type breakdown and analysis for all samples used in this study are presented.

Synthesis and purification of methylglyoxal

MG was purchased from Sigma-Aldrich as a solution at 40 % in H_2O (M0252). This solution was then further purified by steam distillation. The collected fractions were adjusted to pH 7.0 with NaOH and aliquots of them were reacted with H_2O_2 in order to indirectly quantify the pure MG concentration by titration with $KMnO_4$ [76]. Collected fractions were frozen until use.

Acute glycation Mant-ATP chase assay

On the day of experiments, single muscle fibers were dissected and clamped onto cover slips as described above. Fibers were then incubated for five minutes in a modified relaxing buffer solution containing 5.89 mM Na_2ATP, 6.48 mM $MgCl_2$, 40.76 mM propionic acid, 100 mM N,N-Bis(2-hydroxyethyl)-2-aminoethanesulfonic acid sodium salt, 6.97 mM EGTA, 14.5 mM sodium creatine phosphate dibasic and KOH to adjust the pH to 7.1 [77]. After this incubation, fibers then went through

the same protocol as described above of incubation in rigor buffer, Mant-ATP buffer and then fluorescence image acquisition. Following this, the same fibers were incubated in a modified relaxing buffer which contained 50 mM MG for 30 minutes to induce acute glycation of the proteins in these muscle fibers. This buffer contained 5.89 mM Na_2ATP, 6.48 mM $MgCl_2$, 40.76 mM propionic acid, 100 mM N,N-Bis(2-hydroxyethyl)-2-aminoethanesulfonic acid sodium salt, 6.97 mM EGTA, 43.5 mM sodium chloride 50 mM MG and KOH to adjust the pH to 7.4. Following this incubation these muscle fibers were incubated for five minutes in the modified relaxing buffer described above and then went through the exact same process of incubation of in rigor buffer, incubation with Mant-ATP buffer and then fluorescence image acquisition. For analysis purposes the results for each individual muscle fiber were matched before and after MG incubation to observe the effects of acute glycation upon myosin dynamics. All fibers were also stained with *MYH7* to decipher fiber type as described above.

X ray diffraction recordings and analysis

Thin muscle bundles were mounted and transferred to a specimen chamber which was filled with relaxing buffer. The ends of these thin muscle bundles were then clamped at a sarcomere length of 2.00 µm. Subsequently, X-ray diffraction patterns were recorded at 15°C using a CMOS camera (Model C11440-22CU, Hamamatsu Photonics, Japan, 2048 x 2048 pixels) in combination with a 4-inch image intensifier (Model V7739PMOD, Hamamatsu Photonics, Japan). The X-ray wavelength was 0.10 nm, and the specimen-to-detector distance was 2.14 m. For each preparation, approximately 20-50 diffraction patterns were recorded at the BL40XU beamline of SPring-8 and were analysed as described previously [78]. To minimize radiation damage, the exposure time was kept low (0.5 or 1 s) and the specimen chamber was moved by 100 µm after each exposure. Following X-ray recordings, background scattering was subtracted, and the major myosin meridional reflection intensities/spacing were determined as described elsewhere previously [78].

Single Fiber Proteomics

Muscle fiber fragments underwent protein extraction prior sample preparation for proteomics, as previously described [79]. This was achieved by placing the samples in a lysis buffer containing 50 mM Tris buffer at pH 8.5, 1% SDS, 10 mM DTT and 40 mM CAA and boiling for 10 minutes in a thermomixer set at 95℃ with gentle shaking. Next, the samples were sonicated using a bioruptor twin (Diagenode) using a 30 seconds on/off protocol for 15 minutes. Protein lysates were digested into peptides by addition of trypsin (Promega) and LysC (Wako) in an enzyme to protein ratio of 1:100 and 1:500, respectively. The reaction was allowed to take place overnight in a thermomixer set at 37℃ with gentle shaking. The next morning, samples were desalted using SDB-RPS stage-tips crafted in house before loading into Evotips (Evosep), according to the company's sample loading protocol.

Proteomics measurements were conducted using a previously described workflow, in brief: an Evosep One HPLC system (Evosep) coupled via electrospray ionization to a timsTOF SCP mass spectrometer (Bruker) was utilized as the LC-MS system of choice [79,80]. Peptides were separated using the '60 samples per day' chromatographic method before electrospray ionization by a Captive Spray ion source and a 10 µm emitter directly into the MS instrument. Samples were then measured using a DIA-PASEF workflow described elsewhere. Processing of the raw MS spectra was conducted using DIA-NN (version 1.8) in library-based mode, based on an in-house muscle fiber-specific MS library comprising 5000 proteins [81,82]. The DIA-NN settings were as follows: double-pass mode was selected as the neural network mode, the "Robust LC (high accuracy)" was chosen as quantification strategy, prototypic peptides were selected for quantification together with enabling the match between runs option and setting the precursor FDR control to 1%. Unless specified, the other parameters remained as default settings.

Single Fiber Proteomics data analysis/statistical testing

Data analysis was performed using the R software (version 4.3.2) and multiple packages from the R environment. The protein groups matrix was loaded into the software and proteins were log2 transformed before being filtered for at least 70% valid values in at least one of the tested groups (T2DM or control). Next, the filtered protein matrix followed the limma (v 3.54.2) workflow, which included quantile normalization of all samples and differential expression testing between groups in a pseudobulk manner [83]. To adjust p-values for multiple comparison testing, we applied the Benjamini-Hochberg correction for the *type I – type II* comparison, whereas the Xiao significance score was employed for the fiber type-specific comparisons of *controls – T2DM*, which takes into consideration both expression fold change and statistical significance. Therefore, proteins displaying a Xiao score under 0.05 were considered as differentially expressed between groups [84].

Myosin heavy chain band Isolation for post-translational identifications

Briefly, muscle biopsy samples were cut into 15 mg sections. These were immersed into a sample buffer (0.5 M Tris buffer at pH of 6.8, 0.5mg/ml bromophenol blue, 10% SDS, 10% glycerol, 1.25% mercaptoethanol) at 4°C. Samples were then homogenized and centrifuged allowing the supernatant to be extracted and used for SDS-PAGE gels (with stacking gel made with acrylamide/bis 37.5:1 and separation gel made with acrylamide/bis 100:1). Proteins were separated and individual MYH7 band was excised manually [85].

Mass spectrometry-based glycation peptide mapping

SDS-PAGE bands corresponding *MYH7* from control or diabetic groups were subjected to in-gel-digestion. After reduction with DTT (10mM) and alkylation of Cys groups with iodoacetamide (50mM), modified porcine trypsin (Promega) was added at a final ratio of 1:20 (trypsin-protein). Digestion proceeded overnight at 37ºC in 100mM ammonium bicarbonate at pH 7.8. Resulting tryptic peptides were loaded and washed on Evotips and separated in an Endurance 15 cm x 150 µm

ID, 1.9 µm beads-EV1106 column using an Evosep one HPLC system coupled to an Orbitrap Eclipse Tribrid mass spectrometer (Thermo Fisher, San José, CA, USA) and a 30 SPD preprogramed gradient.

MS analysis was performed using the data-independent scanning (DiS) method as described [86], with some modifications. Briefly, each sample was analyzed in a single chromatographic run covering a mass range from 390 to 1000 m/z. The DiS cycle consisted of 255 sequential HCD MS/MS fragmentation events with 2.5 m/z-windows from 390 to 900 m/z, and with 4 m/z-windows from 900 to 1000 m/z. HCD fragmentation was performed using a 33 normalized collision energy. MS/MS scans were performed using 70ms injection time, $3x10^5$ ions AGC target setting and 17,500 resolutions. The whole cycle lasted a maximum of 18 seconds depending on ion intensity during chromatography. The narrow windows used for fragmentation allowed peptide identification using conventional DDA searching algorithms. We used SEQUEST HT as implemented in Proteome Discoverer 2.5 (Thermo Scientific) against a database containing human myosins and with the following parameters: 2 maximum missed trypsin cleavage sites, 3 Da precursor mass tolerance and 30 ppm fragment mass tolerance. Oxidation in Met (+15.995 Da), CEL (+72.021 Da) and Carboxymethyl (+58.005 Da) in Lys, and MG-Hs (+54.011 Da) in Arg were set as variable modifications. Carbamidomethylation (+57.021 Da) in Cys was set as fixed modification [87,88]. To validate and quantify the AGE-modified peptideforms from MYH7 shown in Figure 3b, we used the Vseq application, as described (85). We used the E-score to quantify peptide abundance (85).

Statistical analysis

Data are presented as mean ± standard deviations. Graphs were prepared and analyzed in Graphpad Prism v9. Relevant non-parametric statistical testing was utilized where data was unevenly distributed. Statistical significance was set to $p < 0.05$ unless otherwise stated. Specific statistical tests used are stated in each figure legend.

Data availability

The raw mass spectrometry data are deposited to the ProteomeXchange Consortium via the PRIDE partner repository with the dataset identifier PXD053022 [89].

References

1. Sylow, L., Tokarz, V.L., Richter, E.A., and Klip, A. (2021). The many actions of insulin in skeletal muscle, the paramount tissue determining glycemia. Cell Metabolism *33*, 758-780. 10.1016/j.cmet.2021.03.020.
2. Haselgrove, J.C., and Huxley, H.E. (1973). X-ray evidence for radial cross-bridge movement and for the sliding filament model in actively contracting skeletal muscle. J Mol Biol *77*, 549-568. 10.1016/0022-2836(73)90222-2.
3. Brenner, B., and Eisenberg, E. (1986). Rate of force generation in muscle: correlation with actomyosin ATPase activity in solution. Proc Natl Acad Sci U S A *83*, 3542-3546. 10.1073/pnas.83.10.3542.
4. Harridge, S.D.R., Bottinelli, R., Canepari, M., Pellegrino, M.A., Reggiani, C., Esbjörnsson, M., and Saltin, B. (1996). Whole-muscle and single-fibre contractile properties and myosin heavy chain isoforms in humans. Pflügers Archiv *432*, 913-920. 10.1007/s004240050215.
5. Tokunaga, M., Sutoh, K., and Wakabayashi, T. (1991). Structure and structural change of the myosin head. Advances in Biophysics *27*, 157-167.
6. Gordon, A.M., Homsher, E., and Regnier, M. (2000). Regulation of contraction in striated muscle. Physiol Rev *80*, 853-924. 10.1152/physrev.2000.80.2.853.
7. Stewart, M.A., Franks-Skiba, K., Chen, S., and Cooke, R. (2010). Myosin ATP turnover rate is a mechanism involved in thermogenesis in resting skeletal muscle fibers. Proceedings of the National Academy of Sciences of the United States of America *107*, 430-435. 10.1073/pnas.0909468107.
8. Cooke, R. (2011). The role of the myosin ATPase activity in adaptive thermogenesis by skeletal muscle. Biophysical reviews *3*, 33-45. 10.1007/s12551-011-0044-9.
9. Hooijman, P., Melanie, and Cooke, R. (2011). A New State of Cardiac Myosin with Very Slow ATP Turnover: A Potential Cardioprotective Mechanism in the Heart. Biophysical Journal *100*, 1969-1976. 10.1016/j.bpj.2011.02.061.
10. Grinzato, A., Auguin, D., Kikuti, C., Nandwani, N., Moussaoui, D., Pathak, D., Kandiah, E., Ruppel, K.M., Spudich, J.A., Houdusse, A., and Robert-Paganin, J. (2023). Cryo-EM structure of the folded-back state of human β-cardiac myosin. Nature Communications *14*, 3166. 10.1038/s41467-023-38698-w.
11. Alamo, L., Qi, D., Wriggers, W., Pinto, A., Zhu, J., Bilbao, A., Gillilan, R.E., Hu, S., and Padrón, R. (2016). Conserved Intramolecular Interactions Maintain Myosin Interacting-Heads Motifs Explaining Tarantula Muscle Super-Relaxed State Structural Basis. Journal of molecular biology *428*, 1142-1164. 10.1016/j.jmb.2016.01.027.
12. Toepfer, C.N., Garfinkel, A.C., Venturini, G., Wakimoto, H., Repetti, G., Alamo, L., Sharma, A., Agarwal, R., Ewoldt, J.F., Cloonan, P., et al. (2020). Myosin Sequestration Regulates Sarcomere Function, Cardiomyocyte Energetics, and Metabolism, Informing the Pathogenesis of Hypertrophic Cardiomyopathy. Circulation *141*, 828-842. 10.1161/circulationaha.119.042339.
13. Alamo, L., Ware, J.S., Pinto, A., Gillilan, R.E., Seidman, J.G., Seidman, C.E., and Padrón, R. (2017). Effects of myosin variants on interacting-heads motif explain distinct hypertrophic and dilated cardiomyopathy phenotypes. eLife *6*, e24634. 10.7554/eLife.24634.
14. Craig, R., and Padrón, R. (2022). Structural basis of the super- and hyper-relaxed states of myosin II. Journal of General Physiology *154*. 10.1085/jgp.202113012.
15. Koubassova, N.A., Tsaturyan, A.K., Bershitsky, S.Y., Ferenczi, M.A., Padrón, R., and Craig, R. (2022). Interacting-heads motif explains the X-ray diffraction pattern of relaxed vertebrate skeletal muscle. Biophysical Journal *121*, 1354-1366. 10.1016/j.bpj.2022.03.023.
16. Hooijman, P., Stewart, M.A., and Cooke, R. (2011). A new state of cardiac myosin with very slow ATP turnover: a potential cardioprotective mechanism in the heart. Biophys J *100*, 1969-1976. 10.1016/j.bpj.2011.02.061.

17. Lewis, C.T.A., and Ochala, J. (2022). Myosin as a novel key modulator of striated muscle metabolism. Physiology. 10.1152/physiol.00018.2022.
18. McNamara, J.W., and Sadayappan, S. (2018). Skeletal myosin binding protein-C: An increasingly important regulator of striated muscle physiology. Archives of biochemistry and biophysics *660*, 121-128. 10.1016/j.abb.2018.10.007.
19. Phung, L.A., Foster, A.D., Miller, M.S., Lowe, D.A., and Thomas, D.D. (2020). Super-relaxed state of myosin in human skeletal muscle is fiber-type dependent. American Journal of Physiology-Cell Physiology *319*, C1158-C1162. 10.1152/ajpcell.00396.2020.
20. Toepfer, C.N., Wakimoto, H., Garfinkel, A.C., McDonough, B., Liao, D., Jiang, J., Tai, A.C., Gorham, J.M., Lunde, I.G., Lun, M., et al. (2019). Hypertrophic cardiomyopathy mutations in MYBPC3 dysregulate myosin. Science translational medicine *11*, eaat1199. 10.1126/scitranslmed.aat1199.
21. McNamara, J.W., Li, A., Lal, S., Bos, J.M., Harris, S.P., van der Velden, J., Ackerman, M.J., Cooke, R., and Dos Remedios, C.G. (2017). MYBPC3 mutations are associated with a reduced super-relaxed state in patients with hypertrophic cardiomyopathy. PloS one *12*, e0180064-e0180064. 10.1371/journal.pone.0180064.
22. McNamara, J.W., Li, A., Smith, N.J., Lal, S., Graham, R.M., Kooiker, K.B., van Dijk, S.J., Remedios, C.G.D., Harris, S.P., and Cooke, R. (2016). Ablation of cardiac myosin binding protein-C disrupts the super-relaxed state of myosin in murine cardiomyocytes. Journal of molecular and cellular cardiology *94*, 65-71. 10.1016/j.yjmcc.2016.03.009.
23. Sitbon, Y.H., Kazmierczak, K., Liang, J., Yadav, S., Veerasammy, M., Kanashiro-Takeuchi, R.M., and Szczesna-Cordary, D. (2020). Ablation of the N terminus of cardiac essential light chain promotes the super-relaxed state of myosin and counteracts hypercontractility in hypertrophic cardiomyopathy mutant mice. The FEBS journal *287*, 3989-4004. 10.1111/febs.15243.
24. Trivedi, D.V., Adhikari, A.S., Sarkar, S.S., Ruppel, K.M., and Spudich, J.A. (2018). Hypertrophic cardiomyopathy and the myosin mesa: viewing an old disease in a new light. Biophysical reviews *10*, 27-48. 10.1007/s12551-017-0274-6.
25. Ranu, N., Laitila, J., Dugdale, H.F., Mariano, J., Kolb, J.S., Wallgren-Pettersson, C., Witting, N., Vissing, J., Vilchez, J.J., Fiorillo, C., et al. (2022). NEB mutations disrupt the super-relaxed state of myosin and remodel the muscle metabolic proteome in nemaline myopathy. Acta Neuropathol Commun *10*, 185. 10.1186/s40478-022-01491-9.
26. Thornalley, P.J. (2005). Dicarbonyl intermediates in the maillard reaction. Ann N Y Acad Sci *1043*, 111-117. 10.1196/annals.1333.014.
27. Phillips, S.A., and Thornalley, P.J. (1993). The formation of methylglyoxal from triose phosphates. Investigation using a specific assay for methylglyoxal. Eur J Biochem *212*, 101-105. 10.1111/j.1432-1033.1993.tb17638.x.
28. Dobler, D., Ahmed, N., Song, L., Eboigbodin, K.E., and Thornalley, P.J. (2006). Increased dicarbonyl metabolism in endothelial cells in hyperglycemia induces anoikis and impairs angiogenesis by RGD and GFOGER motif modification. Diabetes *55*, 1961-1969. 10.2337/db05-1634.
29. Nicolay, J.P., Schneider, J., Niemoeller, O.M., Artunc, F., Portero-Otin, M., Haik, G., Jr., Thornalley, P.J., Schleicher, E., Wieder, T., and Lang, F. (2006). Stimulation of suicidal erythrocyte death by methylglyoxal. Cell Physiol Biochem *18*, 223-232. 10.1159/000097669.
30. Aragonès, G., Rowan, S., Francisco, S.G., Whitcomb, E.A., Yang, W., Perini-Villanueva, G., Schalkwijk, C.G., Taylor, A., and Bejarano, E. (2021). The Glyoxalase System in Age-Related Diseases: Nutritional Intervention as Anti-Ageing Strategy. Cells *10*. 10.3390/cells10081852.
31. McLellan, A.C., Thornalley, P.J., Benn, J., and Sonksen, P.H. (1994). Glyoxalase system in clinical diabetes mellitus and correlation with diabetic complications. Clin Sci (Lond) *87*, 21-29. 10.1042/cs0870021.

32. Wang, H., Meng, Q.H., Gordon, J.R., Khandwala, H., and Wu, L. (2007). Proinflammatory and proapoptotic effects of methylglyoxal on neutrophils from patients with type 2 diabetes mellitus. Clinical Biochemistry *40*, 1232-1239. https://doi.org/10.1016/j.clinbiochem.2007.07.016.
33. Ahmed, M.U., Brinkmann Frye, E., Degenhardt, T.P., Thorpe, S.R., and Baynes, J.W. (1997). N-epsilon-(carboxyethyl)lysine, a product of the chemical modification of proteins by methylglyoxal, increases with age in human lens proteins. Biochem J *324 (Pt 2)*, 565-570. 10.1042/bj3240565.
34. Ahmed, N., Thornalley, P.J., Dawczynski, J., Franke, S., Strobel, J., Stein, G., and Haik, G.M. (2003). Methylglyoxal-derived hydroimidazolone advanced glycation end-products of human lens proteins. Invest Ophthalmol Vis Sci *44*, 5287-5292. 10.1167/iovs.03-0573.
35. Brinkmann, E., Wells-Knecht, K.J., Thorpe, S.R., and Baynes, J.W. (1995). Characterization of an imidazolium compound formed by reaction of methylglyoxal and Nα-hippuryllysine. Journal of the Chemical Society, Perkin Transactions 1, 2817-2818. 10.1039/P19950002817.
36. Lederer, M.O., and Klaiber, R.G. (1999). Cross-linking of proteins by Maillard processes: characterization and detection of lysine-arginine cross-links derived from glyoxal and methylglyoxal. Bioorg Med Chem *7*, 2499-2507. 10.1016/s0968-0896(99)00212-6.
37. Khalid, M., Petroianu, G., and Adem, A. (2022). Advanced Glycation End Products and Diabetes Mellitus: Mechanisms and Perspectives. Biomolecules *12*. 10.3390/biom12040542.
38. Papadaki, M., Holewinski, R.J., Previs, S.B., Martin, T.G., Stachowski, M.J., Li, A., Blair, C.A., Moravec, C.S., Van Eyk, J.E., Campbell, K.S., et al. (2018). Diabetes with heart failure increases methylglyoxal modifications in the sarcomere, which inhibit function. JCI Insight *3*. 10.1172/jci.insight.121264.
39. Papadaki, M., Kampaengsri, T., Barrick, S.K., Campbell, S.G., von Lewinski, D., Rainer, P.P., Harris, S.P., Greenberg, M.J., and Kirk, J.A. (2022). Myofilament glycation in diabetes reduces contractility by inhibiting tropomyosin movement, is rescued by cMyBPC domains. J Mol Cell Cardiol *162*, 1-9. https://doi.org/10.1016/j.yjmcc.2021.08.012.
40. Janssens, J.V., Ma, B., Brimble, M.A., Van Eyk, J.E., Delbridge, L.M.D., and Mellor, K.M. (2018). Cardiac troponins may be irreversibly modified by glycation: novel potential mechanisms of cardiac performance modulation. Sci Rep *8*, 16084. 10.1038/s41598-018-33886-x.
41. Thompson, B.R., and Metzger, J.M. (2014). Cell biology of sarcomeric protein engineering: disease modeling and therapeutic potential. Anat Rec (Hoboken) *297*, 1663-1669. 10.1002/ar.22966.
42. Ma, W., Gong, H., and Irving, T. (2018). Myosin Head Configurations in Resting and Contracting Murine Skeletal Muscle. International Journal of Molecular Sciences *19*, 2643. 10.3390/ijms19092643.
43. Deshmukh, A.S. (2016). Proteomics of Skeletal Muscle: Focus on Insulin Resistance and Exercise Biology. Proteomes *4*. 10.3390/proteomes4010006.
44. Lewis, C.T.A., Tabrizian, L., Nielsen, J., Laitila, J., Beck, T.N., Olsen, M.S., Ognjanovic, M.M., Aagaard, P., Hokken, R., Laugesen, S., et al. (2023). Physical activity impacts resting skeletal muscle myosin conformation and lowers its ATP consumption. J Gen Physiol *155*. 10.1085/jgp.202213268.
45. Lewis, C.T.A., Melhedegaard, E.G., Ognjanovic, M.M., Olsen, M.S., Laitila, J., Seaborne, R.A.E., Gronset, M.N., Zhang, C., Iwamoto, H., Hessel, A.L., et al. (2023). Remodelling of Skeletal Muscle Myosin Metabolic States in Hibernating Mammals. Cold Spring Harbor Laboratory.
46. Mengeste, A.M., Rustan, A.C., and Lund, J. (2021). Skeletal muscle energy metabolism in obesity. Obesity (Silver Spring) *29*, 1582-1595. 10.1002/oby.23227.
47. Wing, R.R., Marcus, M.D., Epstein, L.H., and Salata, R. (1987). Type II diabetic subjects lose less weight than their overweight nondiabetic spouses. Diabetes Care *10*, 563-566. 10.2337/diacare.10.5.563.

48. Wang, Z., Lavikainen, P., Wikström, K., and Laatikainen, T. (2024). Trajectories of Body Mass Index and Risk for Diabetes Complications and All-Cause Mortality in Finnish Type 2 Diabetes Patients. Clin Epidemiol *16*, 203-212. 10.2147/clep.S450455.
49. Nogara, L., Naber, N., Pate, E., Canton, M., Reggiani, C., and Cooke, R. (2016). Piperine's mitigation of obesity and diabetes can be explained by its up-regulation of the metabolic rate of resting muscle. Proceedings of the National Academy of Sciences of the United States of America *113*, 13009-13014. 10.1073/pnas.1607536113.
50. Tolkatchev, D., Elnatan, D., Nogara, L., Ly, T., Naber, N., Haak, K., Meech, R., Cooke, R., and Kostyukova, A.S. (2018). Piperine, an alkaloid inhibiting the super-relaxed state of myosin, binds to the myosin regulatory light chain. Archives of biochemistry and biophysics *659*, 75-84. 10.1016/j.abb.2018.09.027.
51. Colson, B.A., Petersen, K.J., Collins, B.C., Lowe, D.A., and Thomas, D.D. (2015). The myosin super-relaxed state is disrupted by estradiol deficiency. Biochemical and biophysical research communications *456*, 151-155. 10.1016/j.bbrc.2014.11.050.
52. Herbison, G.J., Jaweed, M.M., and Ditunno, J.F. (1982). Muscle fiber types. Arch Phys Med Rehabil *63*, 227-230.
53. Bourdeau Julien, I., Sephton, C.F., and Dutchak, P.A. (2018). Metabolic Networks Influencing Skeletal Muscle Fiber Composition. Frontiers in Cell and Developmental Biology *6*. 10.3389/fcell.2018.00125.
54. Daugaard, J.R., Nielsen, J.N., Kristiansen, S., Andersen, J.L., Hargreaves, M., and Richter, E.A. (2000). Fiber type-specific expression of GLUT4 in human skeletal muscle: influence of exercise training. Diabetes *49*, 1092-1095. 10.2337/diabetes.49.7.1092.
55. Albers, P.H., Pedersen, A.J., Birk, J.B., Kristensen, D.E., Vind, B.F., Baba, O., Nøhr, J., Højlund, K., and Wojtaszewski, J.F. (2015). Human muscle fiber type-specific insulin signaling: impact of obesity and type 2 diabetes. Diabetes *64*, 485-497. 10.2337/db14-0590.
56. Stuart, C.A., McCurry, M.P., Marino, A., South, M.A., Howell, M.E., Layne, A.S., Ramsey, M.W., and Stone, M.H. (2013). Slow-twitch fiber proportion in skeletal muscle correlates with insulin responsiveness. J Clin Endocrinol Metab *98*, 2027-2036. 10.1210/jc.2012-3876.
57. Brito, R., Alamo, L., Lundberg, U., Guerrero, J.R., Pinto, A., Sulbarán, G., Gawinowicz, M.A., Craig, R., and Padrón, R. (2011). A molecular model of phosphorylation-based activation and potentiation of tarantula muscle thick filaments. Journal of molecular biology *414*, 44-61. 10.1016/j.jmb.2011.09.017.
58. Dutta, D., Nguyen, V., Campbell, K.S., Padrón, R., and Craig, R. (2023). Cryo-EM structure of the human cardiac myosin filament. Nature *623*, 853-862. 10.1038/s41586-023-06691-4.
59. Allaman, I., Bélanger, M., and Magistretti, P.J. (2015). Methylglyoxal, the dark side of glycolysis. Front Neurosci *9*, 23. 10.3389/fnins.2015.00023.
60. Schalkwijk, C.G., and Stehouwer, C.D.A. (2020). Methylglyoxal, a Highly Reactive Dicarbonyl Compound, in Diabetes, Its Vascular Complications, and Other Age-Related Diseases. Physiol Rev *100*, 407-461. 10.1152/physrev.00001.2019.
61. Du, H., Ma, Y., Wang, X., Zhang, Y., Zhu, L., Shi, S., Pan, S., and Liu, Z. (2023). Advanced glycation end products induce skeletal muscle atrophy and insulin resistance via activating ROS-mediated ER stress PERK/FOXO1 signaling. American Journal of Physiology-Endocrinology and Metabolism *324*, E279-E287. 10.1152/ajpendo.00218.2022.
62. Lee, H.W., Gu, M.J., Lee, J.Y., Lee, S., Kim, Y., and Ha, S.K. (2021). Methylglyoxal-Lysine Dimer, an Advanced Glycation End Product, Induces Inflammation via Interaction with RAGE in Mesangial Cells. Mol Nutr Food Res *65*, e2000799. 10.1002/mnfr.202000799.
63. Schaub, M.C., Hefti, M.A., Zuellig, R.A., and Morano, I. (1998). Modulation of contractility in human cardiac hypertrophy by myosin essential light chain isoforms. Cardiovasc Res *37*, 381-404. 10.1016/s0008-6363(97)00258-7.
64. Wang, T.Y., Arking, D.E., Maleszewski, J.J., Fox-Talbot, K., Nieuwenhuis, T.O., Santhanam, L., Virmani, R., Rosenberg, A.Z., and Halushka, M.K. (2019). Human cardiac myosin light chain 4

(MYL4) mosaic expression patterns vary by sex. Sci Rep *9*, 12681. 10.1038/s41598-019-49191-0.
65. Peng, W., Li, M., Li, H., Tang, K., Zhuang, J., Zhang, J., Xiao, J., Jiang, H., Li, D., Yu, Y., et al. Dysfunction of Myosin Light-Chain 4 (MYL4) Leads to Heritable Atrial Cardiomyopathy With Electrical, Contractile, and Structural Components: Evidence From Genetically-Engineered Rats. Journal of the American Heart Association *6*, e007030. 10.1161/JAHA.117.007030.
66. Saat, H., Şahin, İ., Erdem, H.B., Özgür, S., Terlemez Tokgöz, S., and Bahsi, T. (2022). Molecular Approach of Hereditary Arrhythmias, Long QT Syndrome, and Arrhythmogenic Right Ventricular Cardiomyopathy. Anatol J Cardiol *26*, 460-465. 10.5152/AnatolJCardiol.2022.1324.
67. Bettahi, I., Krishnankutty, R., Jaganjac, M., Suleiman, N.N.M., Ramanjaneya, M., Jerobin, J., Hassoun, S., Alkasem, M., Abdelhakam, I., Iskandarani, A., et al. (2022). Differences in protein expression, at the basal state and at 2 h of insulin infusion, in muscle biopsies from healthy Arab men with high or low insulin sensitivity measured by hyperinsulinemic euglycemic clamp. Front Endocrinol (Lausanne) *13*, 1024832. 10.3389/fendo.2022.1024832.
68. Jové, M., Salla, J., Planavila, A., Cabrero, À., Michalik, L., Wahli, W., Laguna, J.C., and Vázquez-Carrera, M. (2004). Impaired expression of NADH dehydrogenase subunit 1 and PPARγ coactivator-1 in skeletal muscle of ZDF rats: restoration by troglitazone. Journal of Lipid Research *45*, 113-123. https://doi.org/10.1194/jlr.M300208-JLR200.
69. Wirth, C., Brandt, U., Hunte, C., and Zickermann, V. (2016). Structure and function of mitochondrial complex I. Biochim Biophys Acta *1857*, 902-914. 10.1016/j.bbabio.2016.02.013.
70. Öhman, T., Teppo, J., Datta, N., Mäkinen, S., Varjosalo, M., and Koistinen, H.A. (2021). Skeletal muscle proteomes reveal downregulation of mitochondrial proteins in transition from prediabetes into type 2 diabetes. iScience *24*, 102712. 10.1016/j.isci.2021.102712.
71. Chae, S., Kim, S.-J., Do Koo, Y., Lee, J.H., Kim, H., Ahn, B.Y., Ha, Y.-C., Kim, Y.-H., Jang, M.G., Koo, K.-H., et al. (2018). A mitochondrial proteome profile indicative of type 2 diabetes mellitus in skeletal muscles. Experimental & Molecular Medicine *50*, 1-14. 10.1038/s12276-018-0154-6.
72. Søndergård, S.D., Cintin, I., Kuhlman, A.B., Morville, T.H., Bergmann, M.L., Kjær, L.K., Poulsen, H.E., Giustarini, D., Rossi, R., Dela, F., et al. (2021). The effects of 3 weeks of oral glutathione supplementation on whole body insulin sensitivity in obese males with and without type 2 diabetes: a randomized trial. Applied Physiology, Nutrition, and Metabolism *46*, 1133-1142. 10.1139/apnm-2020-1099 %M 33740389.
73. Ochala, J., Finno, C.J., and Valberg, S.J. (2021). Myofibre Hyper-Contractility in Horses Expressing the Myosin Heavy Chain Myopathy Mutation, MYH1E321G. Cells *10*, 3428.
74. Ross, J.A., Pearson, A., Levy, Y., Cardel, B., Handschin, C., and Ochala, J. (2017). Exploring the Role of PGC-1α in Defining Nuclear Organisation in Skeletal Muscle Fibres. Journal of Cellular Physiology *232*, 1270-1274. https://doi.org/10.1002/jcp.25678.
75. Ross, J.A., Levy, Y., Ripolone, M., Kolb, J.S., Turmaine, M., Holt, M., Lindqvist, J., Claeys, K.G., Weis, J., Monforte, M., et al. (2019). Impairments in contractility and cytoskeletal organisation cause nuclear defects in nemaline myopathy. Acta Neuropathol *138*, 477-495. 10.1007/s00401-019-02034-8.
76. Friedemann, T.E. (1927). THE ACTION OF ALKALI AND HYDROGEN PEROXIDE ON GLYOXALS. Journal of Biological Chemistry *73*, 331-334. https://doi.org/10.1016/S0021-9258(18)84316-2.
77. Au - Gonçalves-Rodrigues, P., Au - Almeida-Coelho, J., Au - Gonçalves, A., Au - Amorim, F., Au - Leite-Moreira, A.F., Au - Stienen, G.J.M., and Au - Falcão-Pires, I. (2020). In Vitro Assessment of Cardiac Function Using Skinned Cardiomyocytes. JoVE, e60427. doi:10.3791/60427.

78. Ochala, J., Iwamoto, H., Larsson, L., and Yagi, N. (2010). A myopathy-linked tropomyosin mutation severely alters thin filament conformational changes during activation. Proceedings of the National Academy of Sciences *107*, 9807-9812. doi:10.1073/pnas.1001733107.
79. Moreno-Justicia, R., Stede, T.V.d., Stocks, B., Laitila, J., Seaborne, R.A., Loock, A.V.d., Lievens, E., Samodova, D., Marín-Arraiza, L., Dmytriyeva, O., et al. (2023). Human Skeletal Muscle Fiber Heterogeneity Beyond Myosin Heavy Chains. bioRxiv, 2023.2009.2007.556665. 10.1101/2023.09.07.556665.
80. Bache, N., Geyer, P.E., Bekker-Jensen, D.B., Hoerning, O., Falkenby, L., Treit, P.V., Doll, S., Paron, I., Müller, J.B., Meier, F., et al. (2018). A Novel LC System Embeds Analytes in Pre-formed Gradients for Rapid, Ultra-robust Proteomics. Mol Cell Proteomics *17*, 2284-2296. 10.1074/mcp.TIR118.000853.
81. Meier, F., Brunner, A.D., Frank, M., Ha, A., Bludau, I., Voytik, E., Kaspar-Schoenefeld, S., Lubeck, M., Raether, O., Bache, N., et al. (2020). diaPASEF: parallel accumulation-serial fragmentation combined with data-independent acquisition. Nat Methods *17*, 1229-1236. 10.1038/s41592-020-00998-0.
82. Demichev, V., Messner, C.B., Vernardis, S.I., Lilley, K.S., and Ralser, M. (2020). DIA-NN: neural networks and interference correction enable deep proteome coverage in high throughput. Nat Methods *17*, 41-44. 10.1038/s41592-019-0638-x.
83. Ritchie, M.E., Phipson, B., Wu, D., Hu, Y., Law, C.W., Shi, W., and Smyth, G.K. (2015). limma powers differential expression analyses for RNA-sequencing and microarray studies. Nucleic Acids Res *43*, e47. 10.1093/nar/gkv007.
84. Xiao, Y., Hsiao, T.H., Suresh, U., Chen, H.I., Wu, X., Wolf, S.E., and Chen, Y. (2014). A novel significance score for gene selection and ranking. Bioinformatics *30*, 801-807. 10.1093/bioinformatics/btr671.
85. Andersen, J.L., and Aagaard, P. (2000). Myosin heavy chain IIX overshoot in human skeletal muscle. Muscle & Nerve *23*, 1095-1104. https://doi.org/10.1002/1097-4598(200007)23:7<1095::AID-MUS13>3.0.CO;2-O.
86. Guarás, A., Perales-Clemente, E., Calvo, E., Acín-Pérez, R., Loureiro-Lopez, M., Pujol, C., Martínez-Carrascoso, I., Nuñez, E., García-Marqués, F., Rodríguez-Hernández, M.A., et al. (2016). The CoQH2/CoQ Ratio Serves as a Sensor of Respiratory Chain Efficiency. Cell Rep *15*, 197-209. 10.1016/j.celrep.2016.03.009.
87. Orsburn, B.C. (2021). Proteome Discoverer-A Community Enhanced Data Processing Suite for Protein Informatics. Proteomes *9*. 10.3390/proteomes9010015.
88. Kong, A.T., Leprevost, F.V., Avtonomov, D.M., Mellacheruvu, D., and Nesvizhskii, A.I. (2017). MSFragger: ultrafast and comprehensive peptide identification in mass spectrometry–based proteomics. Nature Methods *14*, 513-520. 10.1038/nmeth.4256.
89. Perez-Riverol, Y., Bai, J., Bandla, C., García-Seisdedos, D., Hewapathirana, S., Kamatchinathan, S., Kundu, D.J., Prakash, A., Frericks-Zipper, A., Eisenacher, M., et al. (2022). The PRIDE database resources in 2022: a hub for mass spectrometry-based proteomics evidences. Nucleic Acids Res *50*, D543-d552. 10.1093/nar/gkab1038.

Acknowledgements

This work was generously funded by the Novo Nordisk Foundation grants (NNF-21OC0070539 and NNF23-OC0085045) and Lundbeckfonden (R434-2023-311) to J.O. The X-ray experiments were under approval of the SPring-8 Proposal Review Committee (2022A1069). Mass spectrometry-based proteomics analyses were performed by the Proteomics Research Infrastructure (PRI) at the University of Copenhagen (UCPH), supported by the Novo Nordisk Foundation (NNF) (grant agreement number NNF19SA0059305). The CNIC is supported by the MCIN, the Instituto de Salud Carlos III, and the Pro-CNIC Foundation and is a Severo Ochoa Center of Excellence (grant number CEX2020-001041-S funded by MCIN/AEI/10.13039/501100011033).

Data Availability

The data that support the findings of this study are available from the corresponding author upon reasonable request.

Author Contributions

CTAL, ASD and JO contributed to the study conception and design. Material preparation, data collection and analysis were performed by CTAL, RMJ, LS, EC, AB, JL, RAES, SL, CZ, HI, VZ, MC, JAM, GG, JAC, TJH, MA and ASD. The first draft of the manuscript was written by CTAL and JO and all authors commented on all versions of the manuscript and approved of the submitted version.

Figure Legends

Figure 1 – Myosin relaxed states are altered in T2DM. a. Representative fluorescence mant-ATP decays from single muscle fibers isolated from control and T2DM skeletal muscle biopsies and measured over 300 seconds. **b-c.** Percentage of myosin heads in the P1/DRX (b) or P2/SRX (c) from single muscle fibers obtained from control and T2DM patients. Values were separated based on each individual fiber was MyHC type I or MyHC type II. **d.** T1 value in seconds denoting the ATP turnover lifetime of the DRX. **e.** T2 value in seconds denoting the ATP turnover lifetime in seconds of the SRX. Grey circles represent the values from each individual muscle fiber which was analyzed. Colored triangles represent the mean value from an individual participant, 8-12 fibers analyzed per participant. Statistical analysis was performed upon mean values. Unpaired student's t-test was used to calculate statistical significance. n = 9-11 participant per group**. f.** Representative x-ray diffraction recordings from permeabilized skeletal muscle bundles from control and T2DM participant. The M3 and M6 meridional reflections are indicated with black arrows. **g.** Normalized intensity (A.U.) of the M3 meridional reflection. **h.** M3 meridional spacing, measured in ångstrom (Å). **i.** Normalized intensity (A.U.) of the M6 meridional reflection. j**.** M6 meridional spacing, measured in ångstrom (Å). Data is displayed as mean ± SEM. Differences were tested using a bilateral Students's t-test. n = 6 participants analyzed per group. * = $p < 0.05$.

Figure 2 – Myosin conformation is unchanged in patients with T1DM. a. Representative fluorescence Mant-ATP decays from single muscle fibers isolated from control and T1DM skeletal muscle biopsies and measured over 300 seconds. **b-c.** Percentage of myosin heads in the P1/DRX (b) or P2/SRX (c) from single muscle fibers obtained from control and T1DM patients. Values were separated based on each individual fiber was MyHC type I or MyHC type II. **d.** T1 value in seconds denoting the ATP turnover lifetime of the DRX. **e.** T2 value in seconds denoting the ATP turnover lifetime in seconds of the SRX. Grey circles represent the values from each individual muscle fiber which was analyzed. Colored triangles represent the mean value from an individual participant, 8-12 fibers analyzed per participant. **f.** Representative X-ray diffraction recordings from permeabilized skeletal muscle bundles from control and T1DM participants. The M3 and M6 meridional reflections are indicated with black arrows. **g.** Normalized intensity (A.U.) of the M3 meridional reflection. **h.** M3 meridional spacing, measured in ångstrom (Å). **i.** Normalized intensity (A.U.) of the M6 meridional reflection. **j.** M6 meridional spacing, measured in ångstrom (Å). Data is displayed as mean ± SEM. n = 5 participants per group. Bilateral Student's t-test was used to assess statistical significance with statistical threshold being set to $p = <0.05$.

Figure 3 – Glycation of type I myosin heavy chain (*MYH7*) in T2DM. a. Schematic of the process of glycolysis from which is formed the intracellular MG and the chemical formulae of some of the MG-derived AGEs that have been detected on different protein residues**. b.** Quantification of several glycated peptides from *MYH7* showing increased glycation in T2DM participants when compared with the controls. Mann-Whitney test was used to calculate statistical significance. * = $p < 0.05$, ** = $p < 0.01$. n = 5 individual participants per group. We could detect several peptide fragments modified through the formation of N^{ε}-(carboxyethyl)lysine (CEL), hydroimidazolones (MG-Hs) or N^{ε}-(carboxymethyl)lysine. **c.** Scheme of *MYH7* protein regions indicating the location of the glycated residues in red. Figure created using BioRender.com.

Figure 4 – Acute glycation increased the percentage of myosin heads in the SRX in control participants.

a. Workflow of loaded Mant-ATP chase experiments in which single muscle fibers were incubated with 50mM MG in between matched experimental runs. Figure created using Biorender.com **b.** Percentage of myosin heads in the P1/DRX before (black circles) and after (red circles) treatment with MG. **c**. or Percentage of myosin heads in the P2/SRX before (black circles) and after (red circles) treatment with MG. Values were separated based on each individual fiber was MyHC type I or MyHC type II. **d.** T1 value in seconds denoting the ATP turnover lifetime of the DRX before (black circles) and after (red circles) treatment with MG. **e.** T2 value in seconds denoting the ATP turnover lifetime in seconds of the SRX before (black circles) and after (red circles) treatment with MG. Values were separated based on each individual fiber was MyHC type I or MyHC type II. Paired Student's t-test was used to calculate statistical significance. * = $p < 0.05$ between fibers before and after MG incubation, Ψ = $p < 0.05$ between groups. n = 5 participants per group.

Figure 5 – Single fiber proteomics shows that type I muscle fibers from T2DM patients have differential expression of sarcomeric proteins.

a. Workflow of the isolation of single skeletal muscle fibers from *vastus lateralis* muscle biopsies and downstream processing of these single muscle fibers using mass spectrometry and subsequent bioinformatics pipeline. Figure created using Biorender.com. **b**. Volcano plot demonstrating differentially expressed proteins between type I and type II muscle fibers from both participant groups. **c**. Volcano plot showing proteins that are differentially expressed in type I fibers between control and T2DM groups. **d**. Volcano plot showing proteins that are differentially expressed in type II fibers between control and T2DM groups. Detailed information of statistical analysis of single fiber proteomics is provided in detail in methods section. n = 5 participants per group.

Table 1 – Subject characteristics for T2DM and matched control subjects. Mean subject characteristics for the participants in the study of which biopsies samples were obtained from. Shown parameters are age (years), BMI (kg/m^2) and MyHC breakdown (%) for all participants. Data is displayed as mean ± SD. Bilateral Student's t-test was used to calculate statistical significance. * = $p<0.05$ between groups. n = 9-11 subjects per group.

	Control	T2DM
Age (Years)	67.9 ± 12.9	67.9 ± 11.4
BMI	29.76 ± 2.7	29.91 ± 2.4
MyHC Type I (%)	50.21 ± 9.46	43.93 ± 12.55
MyHC Type II (%)	49.79 ± 9.46	53.89 ± 12.55*

Table 2 – General characteristics for T1DM and matched control participants. Mean characteristics for the participants in the study of which biopsies samples were obtained from. Shown parameters are sex (M/F), age (years), BMI (kg/m^2) and MyHC breakdown (%) for all participants. Data is displayed as mean ± SD. n = 6 participants per group.

	Control	T1DM
Sex (M/F)	3M/2F	3M/2F
Age (years)	54.2 ± 6.58	53.0 ± 4.15
BMI (kg/m^2)	24.56 ± 1.25	25.38 ± 2.80
MyHC Type I (%)	55.00 ± 16.33	46.67 ± 20.14
MyHC Type II (%)	45.00 ± 16.33	53.33 ± 20.14

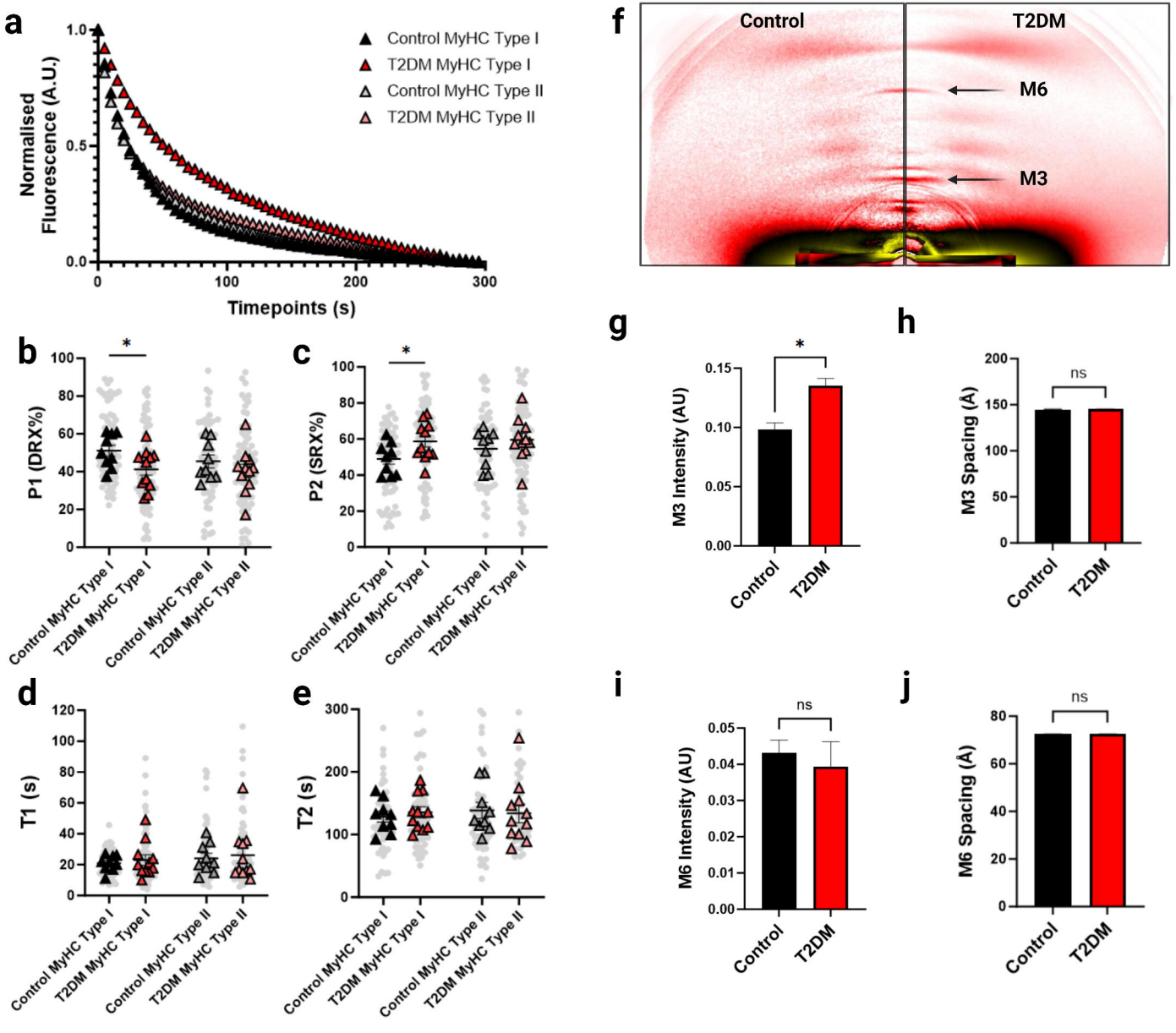
a
Normalised Fluorescence (A.U.)
Timepoints (s)
Control MyHC Type I
T2DM MyHC Type I
Control MyHC Type II
T2DM MyHC Type II
b
P1 (DRX%)
c
P2 (SRX%)
d
T1 (s)
e
T2 (s)
f
Control
T2DM
M6
M3
g
M3 Intensity (AU)
h
M3 Spacing (Å)
i
M6 Intensity (AU)
j
M6 Spacing (Å)
ns
Control
T2DM

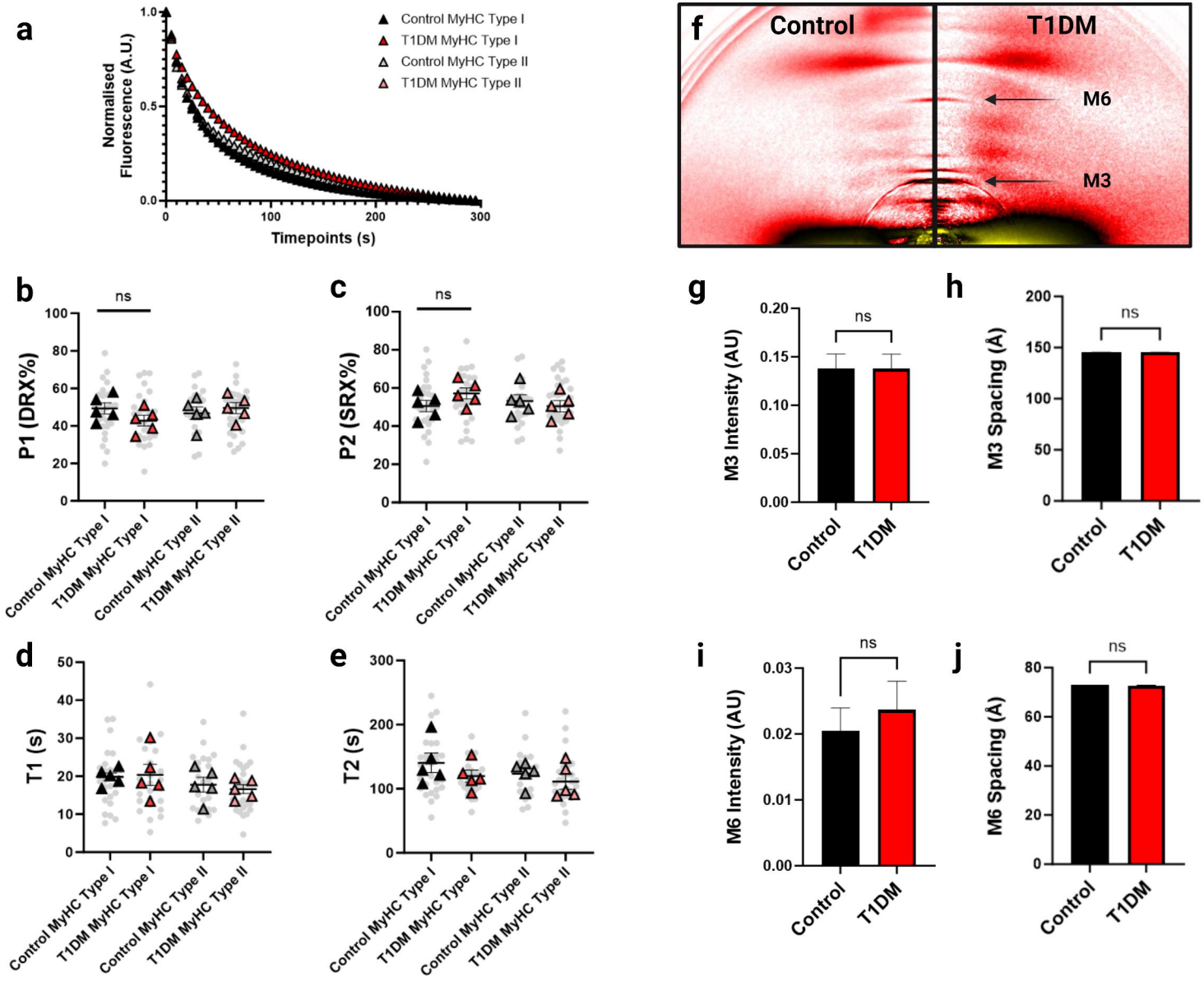
a
Normalised Fluorescence (A.U.)
Timepoints (s)
Control MyHC Type I
T1DM MyHC Type I
Control MyHC Type II
T1DM MyHC Type II
f
Control
T1DM
M6
M3
b
P1 (DRX%)
ns
c
P2 (SRX%)
ns
g
M3 Intensity (AU)
ns
h
M3 Spacing (Å)
ns
d
T1 (s)
e
T2 (s)
i
M6 Intensity (AU)
ns
j
M6 Spacing (Å)
ns
Control MyHC Type I
T1DM MyHC Type I
Control MyHC Type II
T1DM MyHC Type II
Control
T1DM

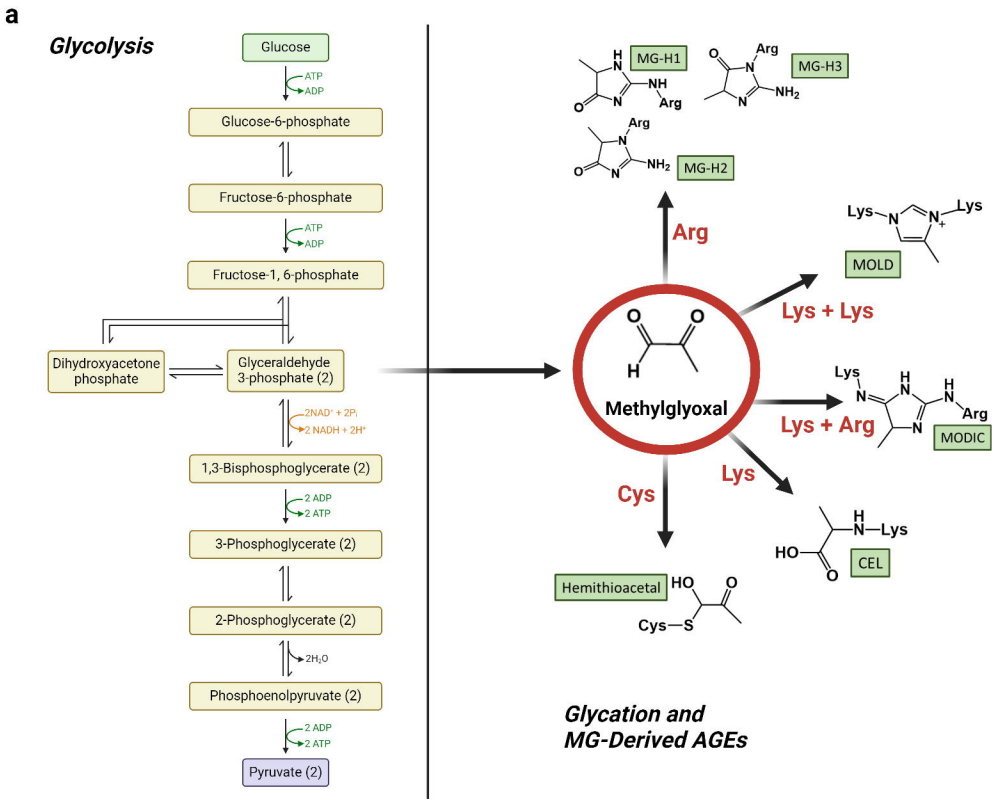
a
Glycolysis
Glucose
ATP
ADP
Glucose-6-phosphate
Fructose-6-phosphate
ATP
ADP
Fructose-1, 6-phosphate
Dihydroxyacetone phosphate
Glyceraldehyde 3-phosphate (2)
2NAD⁺ + 2Pᵢ
2 NADH + 2H⁺
1,3-Bisphosphoglycerate (2)
2 ADP
2 ATP
3-Phosphoglycerate (2)
2-Phosphoglycerate (2)
2H₂O
Phosphoenolpyruvate (2)
2 ADP
2 ATP
Pyruvate (2)
MG-H1
MG-H3
MG-H2
Arg
Lys + Lys
MOLD
Methylglyoxal
Lys + Arg
MODIC
Cys
Lys
CEL
Hemithioacetal
Glycation and
MG-Derived AGEs

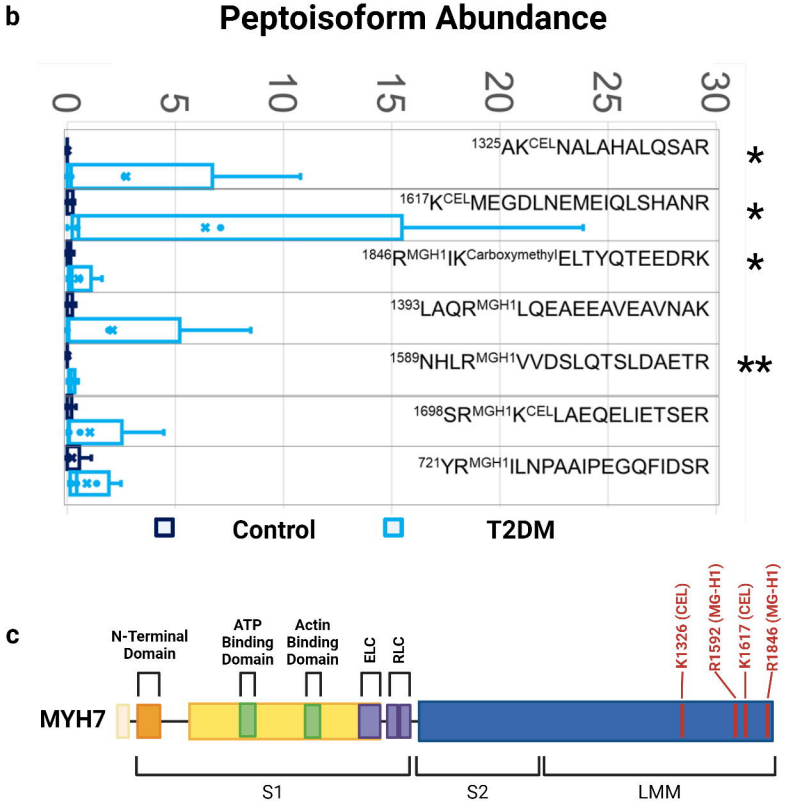
b
Peptoisoform Abundance
0
5
10
15
20
25
30
1325AKCELNALAHALQSAR
1617KCELMEGDLNEMEIQLSHANR
1846RMGH1IKCarboxymethylELTYQTEEDRK
1393LAQRMGH1LQEAEEAVEAVNAK
1589NHLRMGH1VVDSLQTSLDAETR
1698SRMGH1KCELLAEQELIETSER
721YRMGH1ILNPAAIPEGQFIDSR
*
*
*
**
Control
T2DM
c
N-Terminal Domain
ATP Binding Domain
Actin Binding Domain
ELC
RLC
K1326 (CEL)
R1592 (MG-H1)
K1617 (CEL)
R1846 (MG-H1)
MYH7
S1
S2
LMM

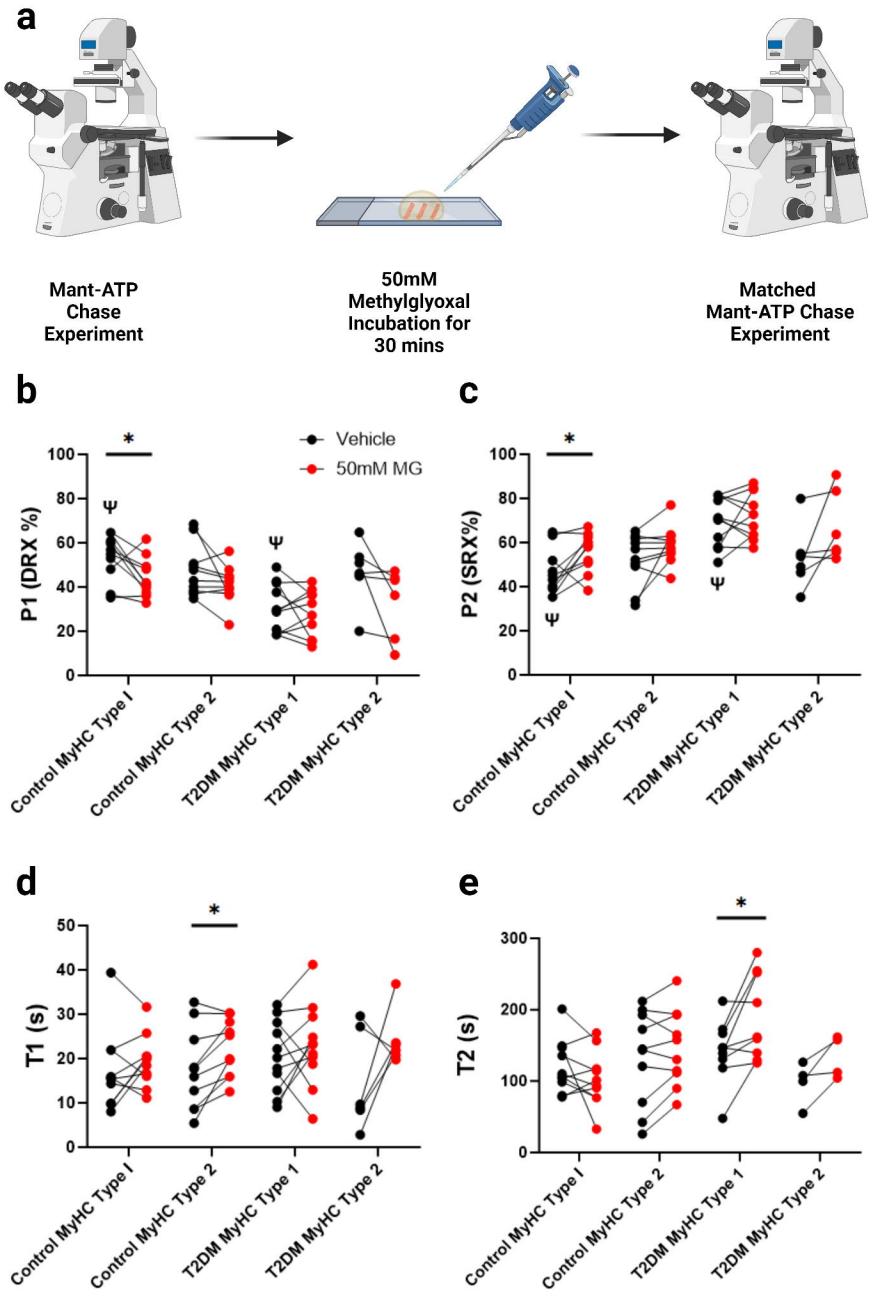
a
Mant-ATP Chase Experiment
50mM Methylglyoxal Incubation for 30 mins
Matched Mant-ATP Chase Experiment
b
Vehicle
50mM MG
P1 (DRX %)
Control MyHC Type I
Control MyHC Type 2
T2DM MyHC Type 1
T2DM MyHC Type 2
c
P2 (SRX%)
d
T1 (s)
e
T2 (s)

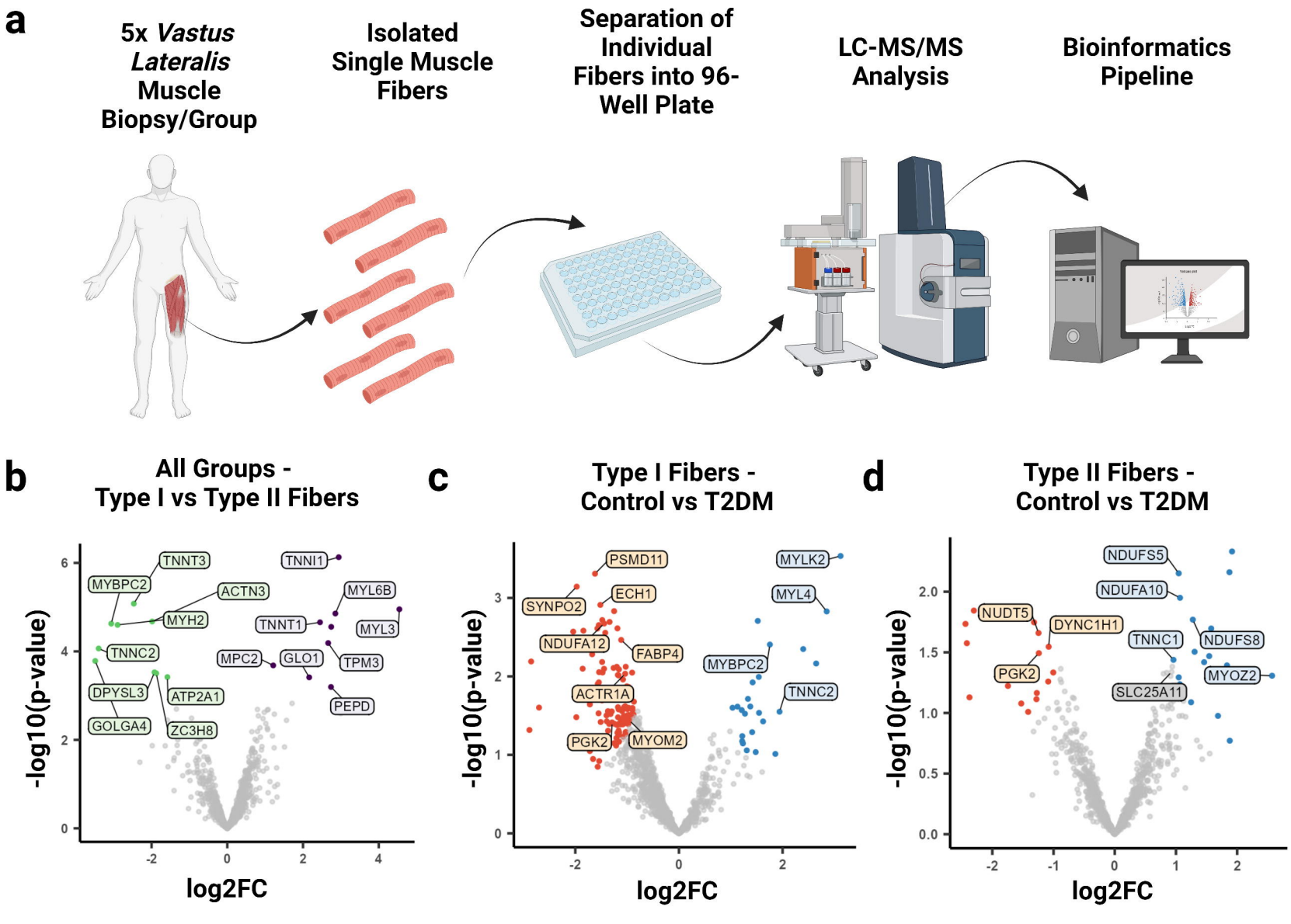
a
5x Vastus Lateralis Muscle Biopsy/Group
Isolated Single Muscle Fibers
Separation of Individual Fibers into 96-Well Plate
LC-MS/MS Analysis
Bioinformatics Pipeline
b
All Groups - Type I vs Type II Fibers
TNNT3
TNNI1
MYBPC2
ACTN3
MYL6B
MYH2
TNNT1
MYL3
TNNC2
MPC2
GLO1
TPM3
DPYSL3
ATP2A1
PEPD
GOLGA4
ZC3H8
-log10(p-value)
log2FC
c
Type I Fibers - Control vs T2DM
PSMD11
MYLK2
SYNPO2
ECH1
MYL4
NDUFA12
FABP4
MYBPC2
ACTR1A
TNNC2
PGK2
MYOM2
-log10(p-value)
log2FC
d
Type II Fibers - Control vs T2DM
NDUFS5
NDUFA10
NUDT5
DYNC1H1
TNNC1
NDUFS8
PGK2
MYOZ2
SLC25A11
-log10(p-value)
log2FC